IGTI/ASME TURBO EXPO 2002
June 2002 Amsterdam The Netherlands

AERODYNAMIC CHARACTER OF PARTIAL SQUEALER TIP ARRANGEMENTS IN AN AXIAL FLOW TURBINE

Part : 2 Detailed Aerodynamic Field Modifications via Three Dimensional Viscous Flow Simulations Around the Baseline Tip

Levent Kavurmacioglu[1], Debashis Dey[2] and Cengiz Camci[3]

Turbomachinery Heat Transfer Laboratory
Department of Aerospace Engineering
The Pennsylvania State University

223 Hammond Building, University Park, PA 16802

ABSTRACT

This paper deals with the viscous flow simulations of the complex tip leakage flow-field existing in the Axial Flow Turbine Facility (AFTRF). Special attention in this part is paid to the 3D structure of the tip leakage flow mechanisms in a baseline tip configuration with no desensitization. The baseline tip flow mechanisms that are already explained from a set of aerodynamic measurements in Part-1 of this paper are visualized in a detailed manner. Although the experimental study presented in Part-1 provides much insight into the physical understanding of the tip region aerodynamics, there are still many areas of the flow-field in which experiments are extremely difficult to perform. Fine details of the entrance flow near the pressure side where the tip leakage jet starts to form, the leakage jet formation between the pressure side and the suction side, the re-circulatory flow zone very near the pressure side corner in the tip gap zone, the interaction area of the tip vortex with the conventional passage vortex system, the influence of the relative motion of the outer casing and leakage flow reversal can all be visualized in great detail by using computational tools solving the three-dimensional Reynolds Averaged Navier-Stokes Equations. The current study uses a two-equation method for the representation of the turbulent flow field. After a brief grid independency discussion, baseline tip predictions are discussed in detail. The current computational results are interpreted with the help of experimental aerodynamic measurements that are presented in Part-1 of this paper. This part of the paper dealing with detailed baseline predictions forms a useful basis for the visualizations that are presented for partial squealer tip configurations in Part-3.

NOMENCLATURE

c	Rotor axial chord length at tip = 0.129 m
BS100	Baseline tip configuration with no tip treatment, full cover , t/h=1.03 % and s=0 mm.
	full cover , t/h=0.33 % and s=0 mm.
C_p	Static pressure coefficient $C_p = \left(p - p_{ref}\right) / 0.5\rho\, W_{inlet}^2$
ε	Turbulent dissipation rate
h	Rotor blade height = 0.123 m
k	Turbulent kinetic energy $k = \overline{u_i u_i} / 2$
κ	Von Karman constant
p_o	Total pressure
p_{atm}	Ambient pressure (also p_{ref})
p_{in}	Inlet total pressure
p	Static pressure
PS, SS	Pressure side, suction side
Re	Reynolds number
ρ	Density
r/h	Non-dimensional radial position measured from hub surface (also y/h in contour plots)
t	Rotor tip clearance height on the part without a squealer rim (baseline)
TE	Trailing edge
U_i	Mean velocity components
U_m	Mean wheel speed at rotor mid-span
τ_{max}	blade maximum thickness
ν	Absolute velocity
W	Relative velocity with respect to turbine rotor
x,y,z	Coordinate system for the numerical analysis (axial, tangential, radial direction in the linear cascade arrangement for computations)
X,Y,Z,T	Flow visualization planes used for numerical laser sheet visualizations (see Figure 7)
z/t	distance between the plane of visualization and the tip platform (see Figures 6)

INTRODUCTION

Tip Clearance Flow: The spacing required between the tips of blades and the stationary casing of an axial flow turbine is a significant source of inefficiency. The leakage flow induced by the pressure differential between the pressure side and suction side of a rotor tip section usually rolls into a

[1] *Visiting Professor*
[2] *Research Assistant*
[3] *Professor of Aerospace Engineering , c-camci@psu.edu*[1]

streamwise vortical structure. Total pressure losses of this passage flow structure measured at the exit of a turbine stage are directly proportional with the tip gap distance. The leakage flow mixing with the rotor passage flow causes total pressure loss and significantly reduces turbine stage efficiency.

Tip leakage related losses might account for as much as a third of the total losses in a stage. Because of the extremely small length scales involved and highly complex 3D, viscous, unsteady, turbulent flow structures, tip gap flows have always been challenging to turbomachinery researchers. Turbine tip gap leakage fluid passes through tip gap region without experiencing a significant expansion and cooling that is typical in the core section of the turbine passage. The leakage fluid with relatively high total temperature flowing through turbine tip gaps can create important turbine durability and endurance problems.

Although there are many past experimental studies aimed at understanding the physical reasons governing the tip vortex flow and heat transfer problem, there is still a need for reasonably accurate three dimensional viscous flow simulations in this region. A computational visualization system used in the tip vortex problem is attractive because of its ability to visualize local flow details that are extremely difficult to measure in inherently tight and 3D tip gap region.

Flow Visualizations via Computations: A numerical simulation of compressible flow near a turbine tip gap region in a linear cascade arrangement was presented by Liu and Bozzola [1]. A significant reduction of gap exit leakage mass flux rate for the case of a moving outer casing was presented when compared to a stationery outer wall. Basson and Lakshminarayana [2] implemented an embedded grid generation method into a three dimensional pressure based semi-implicit scheme for the prediction of tip clearance flows. Sell, Treiber, Casciaro and Gyarmathy [3] presented computational tip aerodynamics results from a linear turbine cascade with an exit Mach number of 0.5. They reported that the computational simulations agree well with their measurements. The effect of tip clearance height and outer casing relative motion in axial flow turbines were investigated by Tallman and Lakshminarayana [4,5] . They reported that the structure of aerothermal losses in the turbine passage change dramatically when the outer casing motion was incorporated into the analysis. Ameri et al. [6] computationally investigated the effect of tip recess on tip heat transfer and efficiency. They found that the numerical prediction of the effect of the casing recess on blade and tip heat transfer and efficiency was reliable.

Bunker, Bailey and Ameri [7] obtained tip heat transfer and pressure measurements in a three bladed linear cascade simulating the first stage blade geometry on a large power generating turbine with flat and smooth tip surfaces. They noticed a central “sweet spot” of low heat transfer extending into the mid chord region and toward the suction side. Measured surface heat transfer coefficients increased 10-20 % when free stream turbulence intensity level was increased from 5 to 9 %. When the sharp tip edge was rounded, the tip heat transfer increased by about 10 %, presumably due to higher allowed tip leakage flow. Bunker and Ameri [8] also published the results of a study dealing with the numerical prediction of the tip gap heat transfer problem defined in [7]. The casing upstream of the blade was recessed. The numerical results with a radiused-edge blade agreed better with the experimental data. They attributed this feature to the absence of a separation bubble in the gap region. Lin, Shih, Chyu and Bunker [9] studied the effects of gap leakage on fluid flow in a contoured turbine nozzle guide vane in a computational study. A numerical analysis of tip vortex flow in an annular turbine

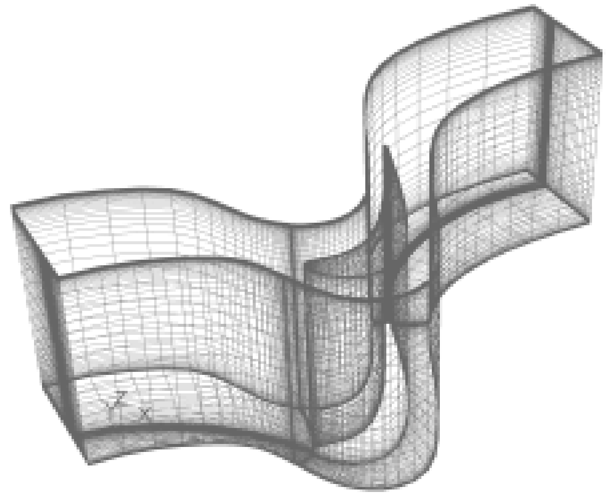

Figure 1, 3D computational grid for the AFTRF turbine rotor flow simulations

cascade configuration was performed by Han, Han, Jin and Goldstein [10]

Current objectives: The present investigation deals with the aerodynamic visualization of tip leakage flow existing in the baseline tip configuration of the (AFTRF) The computational visualizations obtained from three dimensional turbulent flow simulations using a general purpose RANS solver are interpreted using recent aerodynamic field measurements presented in Part-1. The details of the turbine facility and the recent measurements in a naseline tip configuration are presented in Lakshminarayana, Camci, Halliwell & Zaccaria [11] and Dey, Kavurmacioglu & Camci [12], respectively. The comparisons of the numerically visualized tip gap flow field to measured aerodynamic field in the turbine suggest that RANS simulations can be extremely effective in explaining local three dimensional flow field details in turbine flow zones in which aerodynamic measurements are extremely difficult to perform. Numerically generated “*surface oil flow visualizations*” on the tip surface and numerically generated “*vortical flow details*” on user

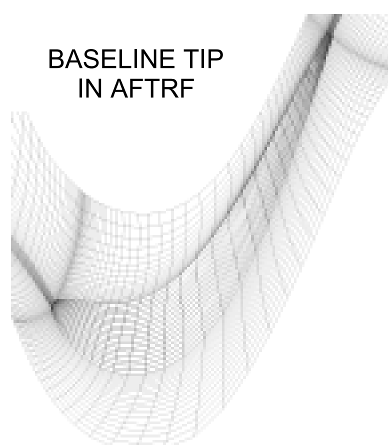

Figure 2, Grid structure near the baseline tip tip configuration

defined planes can be effectively used to discuss local tip flow physics. The "vortical flow details" in user-defined planes are numerical equivalent of "laser sheet visualizations" frequently used in wind tunnel studies. The study clearly shows that the turbine tip gap region includes many different leakage flow regimes depending upon the effective tip clearance, local loading conditions and the rotational speed of the rotor.

NUMERICAL ANALYSIS

Governing Equations: The numerical simulations of the steady-state 3D flow field inside the turbine rotor passage with tip clearance are obtained by solving the three dimensional and incompressible Reynolds Averaged Navier-Stokes equations. A 3D linear cascade equivalent of the annular turbine blade passage is used as shown in Figure 1. The continuity equation and momentum equations in this model are :

$$U_{i,i} = 0 \quad , \tag{1}$$

and $$\rho U_j \frac{\partial U_i}{\partial x_j} = -\frac{\partial p}{\partial x_i} + \mu \frac{\partial^2 U_i}{\partial x_j \partial x_j} + \frac{\partial R_{ij}}{\partial x_j} \tag{2}$$

where $R_{ij} = -\rho \overline{u_i u_j}$ are the Reynolds Stresses. The Reynolds stresses are modeled by using the Boussinesq hypothesis.

$$R_{ij} = -\rho \overline{u_i u_j} = -\rho \frac{2}{3} k \delta_{ij} + \mu_t \left(\frac{\partial U_i}{\partial x_j} + \frac{\partial U_j}{\partial x_i} \right) \tag{3}$$

For two-equation models, the turbulent viscosity is related to turbulent kinetic energy $k = \overline{u_i u_i} / 2$ and the dissipation rate ε as $\mu_t = \rho\, C_\mu\, k^2/\varepsilon$. The turbulent kinetic energy equation is as follows,

$$\rho U_i \frac{\partial k}{\partial x_i} = \mu_t \left(\frac{\partial U_j}{\partial x_i} + \frac{\partial U_i}{\partial x_j} \right) \frac{\partial U_j}{\partial x_i} + \frac{\partial}{\partial x_i} \left\{ (\mu + \mu_t / \sigma_k) \frac{\partial k}{\partial x_i} \right\} - \rho \varepsilon \; . \tag{4}$$

The dissipation rate equation is,

$$\rho U_i \frac{\partial \varepsilon}{\partial x_i} = C_{1\varepsilon} \frac{\varepsilon}{k} \mu_t \left(\frac{\partial U_j}{\partial x_i} + \frac{\partial U_i}{\partial x_j} \right) \frac{\partial U_j}{\partial x_i} - C_{2\varepsilon} \frac{\varepsilon^2}{k} + \frac{\partial}{\partial x_i} \left\{ (\mu + \mu_t / \sigma_\varepsilon) \frac{\partial \varepsilon}{\partial x_i} \right\} \tag{5}$$

where

$$\sigma_{k} = 1, \quad \sigma_\varepsilon = 1.3, \quad C_{1\varepsilon} = 1.44, \quad C_{2\varepsilon} = 1.92$$

are empirical constants.

Near Wall Modeling: The most widely utilized wall functions based on Launder and Spalding [13] are used for the near wall treatment. The law-of-the-wall for mean velocity is,

$$\frac{U_p C_\mu^{1/4} k_p^{1/2}}{\tau_w / \rho} = \frac{1}{\kappa} Ln\left(E y_p^* \right) \tag{6}$$

where $y_p^* = \rho\, C_\mu^{1/4} k_p^{1/2} y_p / \mu$ and (y_p, k_p) are the normal distance from wall to cell center and turbulent kinetic energy at wall-adjacent cell, respectively. The law-of-the-wall for mean velocity is based on wall unit y^* instead of $y^+ = \rho u_\tau y/\mu$ since these are approximately equal to each other in equilibrium turbulent boundary layers.

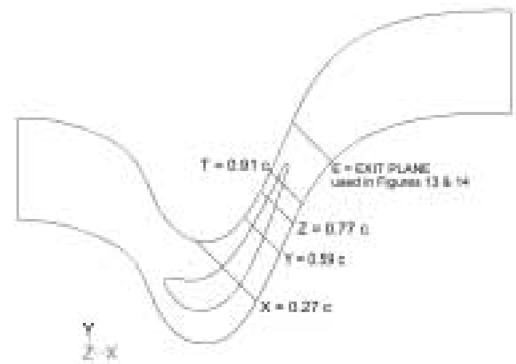

Figure 3 Tip leakage visualization planes (cross-stream direction & blade height)

Method of Solution: The numerical solutions of equations 1 through 5 with proper boundary conditions were carried out by using a finite volume technique based on Fluent 5.5. QUICK discretization scheme was preferred for improved accuracy. SIMPLEC algorithm was selected for the pressure-velocity coupling in order to improve convergence for such a complicated turbulent flow. A multi-grid scheme was used to solve the discretized equations in order to accelerate the convergence of the solver.

Boundary Conditions: All of the computations are performed for Re=291,000 that are based on axial chord length at the tip diameter and mass averaged relative inlet velocity to the rotor passage in the turbine facility. The specific relative velocities from the velocity triangles of the AFTRF rotor described in Part-1 of this paper are used. Figure 4 shows the measured and design values of the axial, tangential and radial velocity components measured just upstream of the turbine rotor in AFTRF. The velocity magnitude and boundary layer profiles at the *"inlet section"*

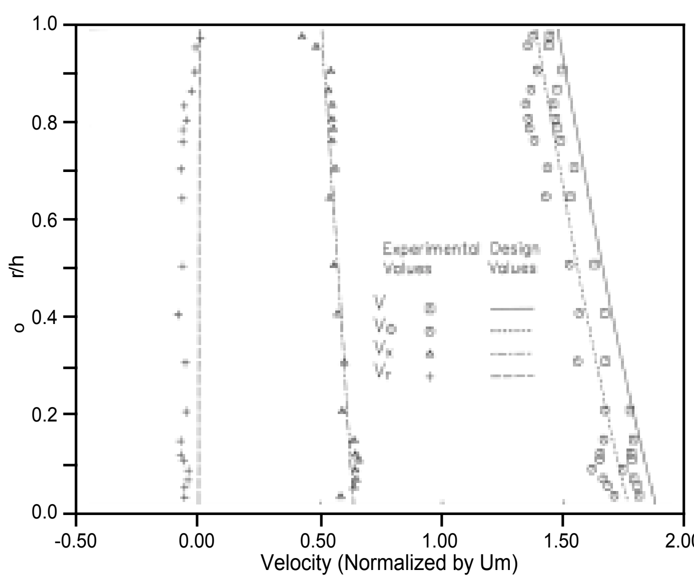

Figure 4, Turbine rotor inlet flow conditions (measured and design values for AFTRF)

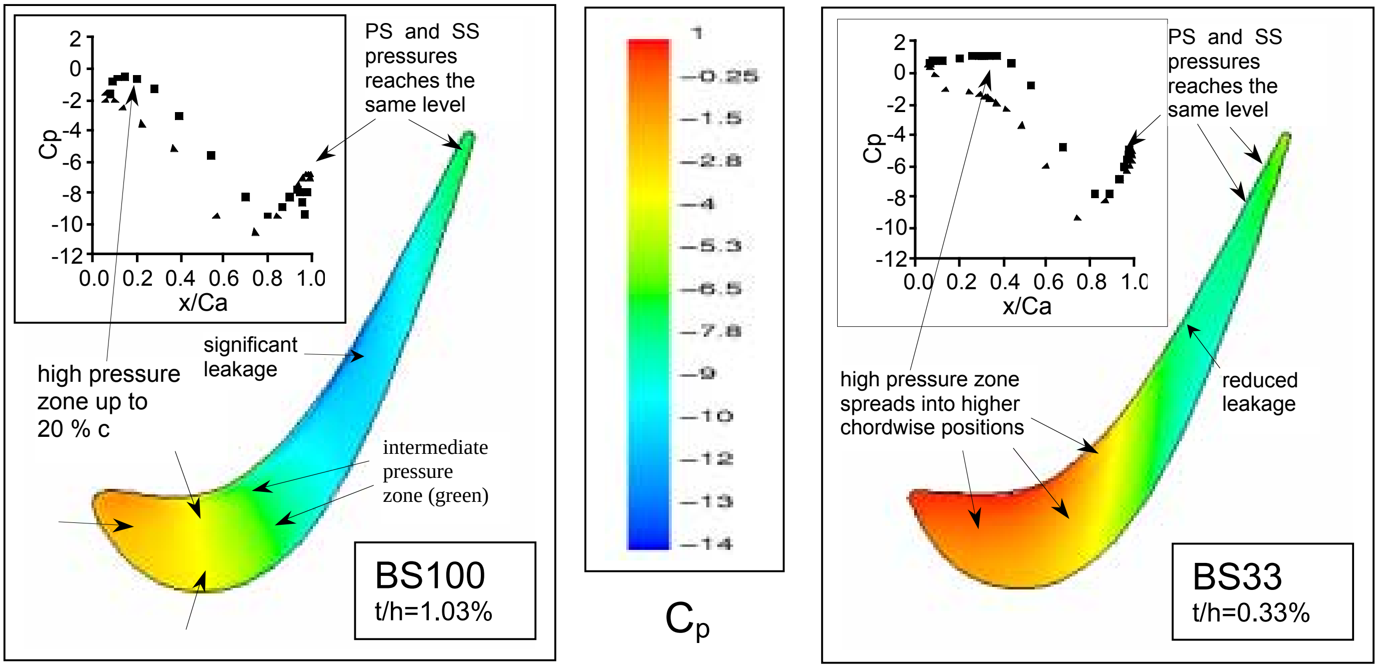

Figure 5, Static pressure distribution on the tip surface of the blade (BASELINE TIP-full cover)

of the three-dimensional computational domain shown in Figure 1 are specified in such a way that the calculated flow direction and magnitude " just upstream of the turbine rotor reasonably represents the tip velocity triangles of the rotor in AFTRF. The values of k and ε that are imposed at the inlet boundary are based on measured turbulence intensity $Tu_\infty = \sqrt{2k/3}/U_\infty$ and length scale defined as $L = C_\mu k_p^{3/2}/\varepsilon$. The measured values of Tu_∞ and L from the AFTRF are used.

Velocities, turbulent kinetic energy and the dissipation rate are all set to zero on solid boundaries except outer casing. The tangential velocity of outer casing that is used for the simulation of casing relative motion is set to a constant. The relative velocity of the outer casing in tangential direction is computed from the turbine rotational speed (N=1320 rpm) at the outer casing diameter (D=0.914 m).

The outlet boundary is set at a sufficient distance from the trailing edge to ensure that there is no influence of the outlet boundary on the flow structure inside the domain. The streamwise gradients of all variables are set to zero for outlet boundary conditions. The steady mean flow through an axial turbomachinery blade row can be modeled as periodic in the circumferential direction. Figure 1 shows the periodic boundaries of the domain in circumferential direction in three dimensional space.

Grid Structure: The grid structure shown in Figures 1 and 2 was generated using a grid-generating program known as GAMBIT. Two different block structured grids that have 130x65x88 points (*fine mesh*) and 105x51x74 points (*medium mesh*) in axial, pitchwise and spanwise directions were generated after initial experiments with a relatively coarser grid. The grid was clustered near the leading, trailing edges and near the tip region when squealer rims were utilized (Part-3). Grid spacing along the spanwise direction was set to obtain an adequate y^+ value near the hub, blade tip surface and casing. The flow field results obtained from the medium mesh and fine mesh were almost identical at the blade mid span location. Figure 2 shows a typical grid structure used for the tip region without a partial squealer rim. 75x65x26 and 50x51x26 grid points were used for the fine mesh and medium mesh inside the tip region respectively. The numerical results were displayed on planes that are almost normal to the turbine blade. The plane definitions in the computational domain are defined in Figure 3.

RESULTS FROM THE BASELINE TIP CONFIGURATION

Static Pressure Field on the Baseline Tip Platform: Figure 5 shows the static pressure distribution on the baseline tip platforms BS100 and BS33 without any squealer rims. The non-dimensional tip gap for BS100 is t/h=1.03 %. The tip gap for BS33 is one third of that of BS100. BS 100 forms the largest tip gap studied in this investigation. BS33 is the minimum tip gap used for a comparative study. The C_p distribution for BS100 shows a (red-yellow) "high pressure zone" in the first 20 % chord distance measured from the leading edge. Between 20 and 35 % chord distance, a green intermediate pressure zone appears just before the portion of the blade where there is a significant amount of leakage flow from the pressure side to the suction side of the blade. The dark blue C_p zone marks the "*dominant leakage zone*" in which most of the fluid leaking from the pressure side to suction side is contained (blue zone). The last 20 % chord of the blade is dominated by a "relatively low leakage zone" as marked by the green zone in BS100. The insets in Figure 5 show the C_p line distribution on the suction side and pressure side of the tip platform. The free stream velocities on both the pressure side and suction side of the blade reach to almost identical levels resulting in very similar chordwise C_p distributions on both sides of the blade in the last 20 % chord.

BS33 presented in Figure 5 shows the spread of the red-yellow "high pressure" zone up to the first 40 % chordwise distance from the leading edge. Since the tip gap is one third of that of BS100, the low momentum fluid contained in this area is not expected to generate a significant leakage flow into the suction side. Relatively low fluid velocities are expected in this zone. The static pressure level indicated by green after the first 40 % chord is not as low as the case BS100. A reduced

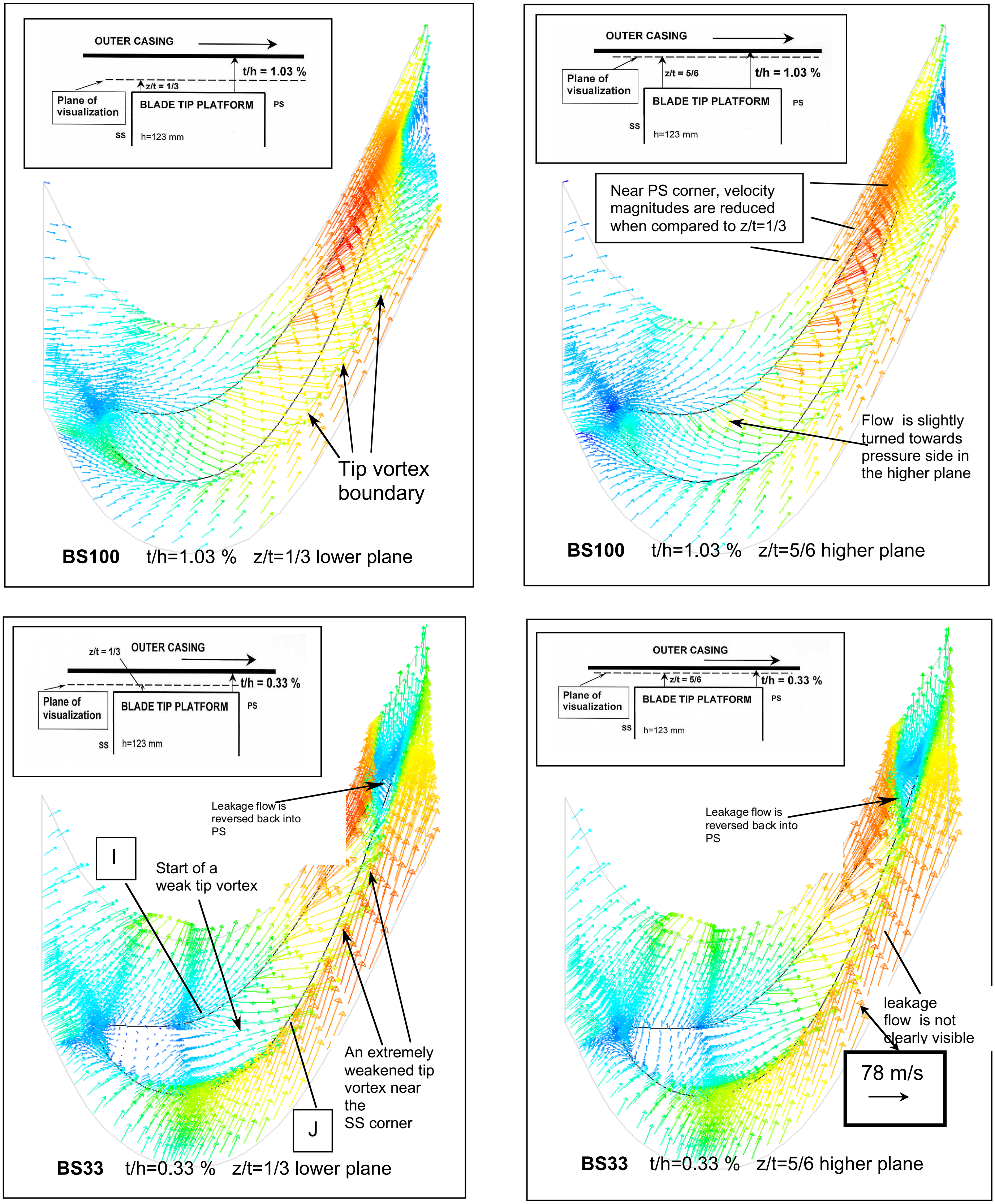

Figure 6, Velocity vectors at various planes in the tip gap (BASELINE TIP - full cover) leakage consistent with this elevated pressure region (green) is expected in BS33. The narrow baseline gap also shows a gradual increase in C_p in the last 20 % chord distance near the trailing edge. The insets in Figure 5 clearly show that the pressure differential between the suction side and pressure side is minimal in this zone.

Velocity Field in Planes Parallel to Baseline Tip Surface: Figure 6 shows the velocity vectors in two selected planes parallel to the blade tip platform. z/t=1/3 "*lower plane*" plane contains the velocity vectors near the tip platform mainly dominated by the pressure driven flow. z/t=5/6 "*higher plane*" shows the velocity vectors in a plane very close to the outer casing that is inducing a significant shear effect on the leakage flow in the gap. For the baseline case BS100 the general trends in terms of the velocity magnitude and direction are similar in the lower plane and higher plane. Near the blade tip platform, most of the flow originating near the pressure side corner tends to pass to the suction side. The strongest leakage velocities are observed as orange-red vectors near the pressure side corner, after 40 % chord distance from the leading edge. The fluid particles from the passage accelerate into the tip gap. The leakage flow vectors in the last 20 % chord are not significant in the trailing edge wedge zone. Although the velocity magnitudes are not small in this zone, the velocity direction is in blade camber-line direction and this flow does not actively participate in the formation of the loss generating vortical system termed as tip vortex in the passage. When one moves to higher plane near the outer casing, a qualitatively similar flow picture is evident This outer casing influence in general works against the leakage flow in the tip gap. The upper right figure in Figure 6 clearly shows the slight turning of the velocity vectors towards the pressure side. This turning is less severe in locations where the pressure difference between the pressure side and the suction side is strong. The turning of the vectors because of the outer casing influence is more significant in regions where the driving pressure difference is minimal between the PS and SS. The leading edge and the last 20 % chord of the blade significant turning of the flow in the upper plane is apparent.

The lower left and right frames in Figure 6 show the velocity vectors when the tip gap is small (t/h=0.33%). The most apparent observation is the dramatic influence of the outer casing motion that is felt equally in both lower visualization plane and upper plane because of the tight clearance. When compared to BS100, the velocity vectors in the planes of the narrow gap termed BS33, there is at least 20 ^{o} to 30 ^{o} directional change towards the pressure side (a counter clockwise turn). When the leakage flows form in the narrow gap, the outer casing has a tremendous ability to pull the fluid layers in a direction opposite to the typical leakage direction. It is interesting to note that the high pressure zone indicated by a red-yellow color in Figure 5 contains an extremely low momentum fluid in the first 20 % of the chord length. The leakage flow in this region is from the suction side to pressure side at a very low velocity. The suction side of the blade does not contribute to a strong tip vortex formation. The boundary IJ for the lower plane in BS33 marks the location where the leakage to the suction side is initiated. Some of the fluid entering from the suction side may travel inside the tip gap for a while before it joins the weak tip vortex formation at about 25 % chord distance just before point J.

Near the trailing edge, the leakage direction is clearly reversed. Because of the extremely narrow tip gap, in the trailing edge region where there is almost no leakage potential for leakage, the tip gap flow is severely turned back into the pressure side of the channel via turbulent shear action. A comparison of BS100 and BS 33 shows a dramatic weakening of the tip vortex by just designing the tip gap in an extremely tight manner. Although not practical for daily turbine operation, BS33 forms a baseline case for comparative purposes in this study. It is expected that when the tight clearance of BS33 is used only in a very narrow region on top of a partial squealer rim, similar flow physics (outer casing shear effect) should contribute to the de-sensitization process.

Recirculatory Tip Flow Patterns in Cross-stream Planes: Figure 7 shows numerically generated flow visualizations inside planes (X,Y,Z and T) defined by the cross stream direction and radial direction. The visualization were generated by drawing pathlines using the velocity components inside the visualization planes. This type of numerical visualization is equivalent to smoke flow visualizations performed in laser sheets of visible light in wind tunnels. A clear leakage flow from the pressure side to suction side is apparent for the baseline gap BS100 at plane X (0.27 % c). The outer casing effect in this zone is not detectable. Most of the fluid leaking in this zone approaches the pressure side corner in a radially outward direction.. An extremely small separation bubble is expected near the pressure side corner. In plane Y (0.59 % c), Leakage flow character is the same as X, however, the tip vortex on the suction side starts growing at a faster rate. Plane Z (0.77 % c) is interesting because of the start of a major directional change of the velocity vectors trying to turn into the pressure side. The leakage flow suddenly looses its driving pressure differential in the last 20-25 % of the trailing edge as shown in the C_p distributions of Figure 5. The turbulent shear action in this region starts pulling some of the tip gap fluid back to the pressure side in region M. A counter clockwise vorticity is induced near the pressure side of the gap. In addition to some weak leakage to the suction side, a highly circulatory bubble (M) forms in the gap. In plane T that is located in the last 10 % of the chord, this flow reversal process is complete. A full reversal of the leakage flow from the suction side to pressure side is observed. Some of the fluid trapped inside the tip vortex structure near the suction side (N) can go back to the tip gap region, eventually crossing to the pressure side of the passage.

The right hand side column in Figure 7 shows the pathlines inside the visualization planes for the small tip gap termed as BS33, t/h=0.33 %. In plane X, although the gap is extremely tight, a weak leakage originates from the pressure side to suction side. The tip vortex keeps growing extremely slowly compared to BS100 as one moves to the trailing edge. The cross section of the leakage vortex near the suction side is much smaller than the case for BS100. The leakage flow is completely reversed in plane Z showing the strong viscous/turbulent shear effect imposed by the outer casing in a zone where the pressure differential between the pressure side and suction side starts to diminish. If the visualization plane Z for BS100 is examined, it is noticed that only a partial reversal to pressure side is apparent. The viscous/turbulent shearing effect of the outer casing starts dominating at a much faster rate when the clearance is tight.

There is a remnant of the original counter clockwise rotating "weak" tip vortex (formed previously), near the suction side corner in plane Z . In plane T, the tip gap flow is completely reversed from the suction side to pressure side. At this location very near the trailing edge, the original "weak" tip vortex is not visible anymore. A slight curvature of the pathlines near the suction side corner is all that is visible. Figure 7 clearly demonstrates the de-sensitization of a large tip vortex area that may contain a tremendous momentum deficit and energy loss in the turbine passage by just reducing the tip gap space.

Leakage Flow Patterns in Planes Parallel to Tip Surface: Figure 8 shows the pathlines for tip gap flows in two different planes (z/t=1/3 and 5/6) for the baseline cases of

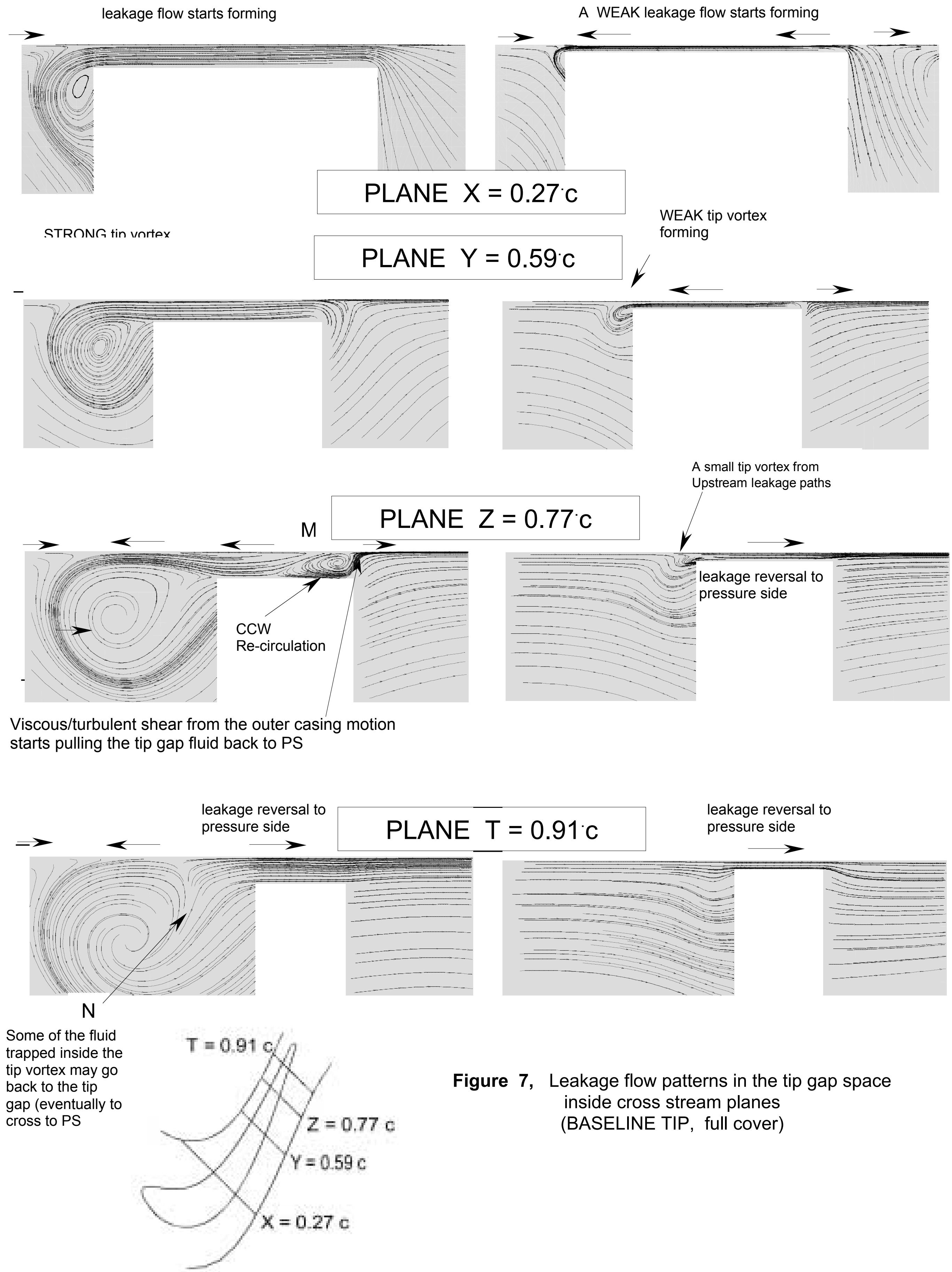

Figure 7, Leakage flow patterns in the tip gap space inside cross stream planes (BASELINE TIP, full cover)

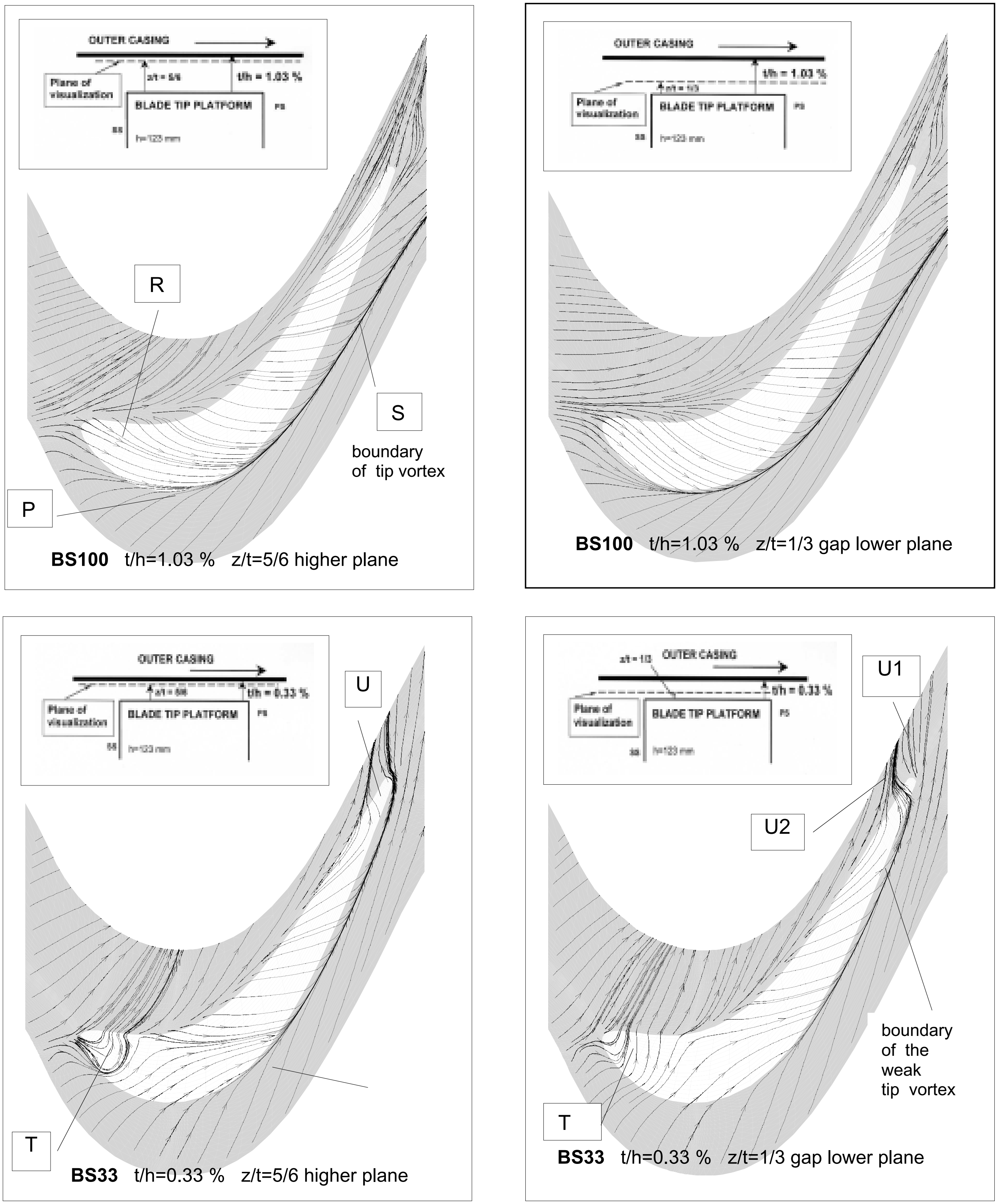

Figure 8, Leakage flow patterns in planes parallel to the tip surface, (BASELINE TIP, full cover)

BS100 and BS33. The fluid particles entering the tip gap space on the suction side near the leading edge follow a path either very close to the blade boundary near the suction side (P) or in the middle section (R) of the leading edge before the location X=0.27.c. The leakage paths for the particles originating from the pressure side corner are well defined. The particles tend to form a clear boundary for the tip vortex in the passage (S). The pathlines are only slightly different in the higher plane at z/t=5/6 (upper-left frame) because of the outer casing pulling effect via viscous/turbulent shear in a direction opposite to a typical leakage direction. The pathlines in the first 1/3 of the blade slightly turn towards the pressure side in the higher plane.

When the tip gap is small, a leading edge and trailing edge modification of leakage flows occur due to the outer case motion in regions where driving pressure differentials are small. In both the lower and higher visualization plane in Figure 8, the fluid from the suction side crosses the gap in a direction towards the pressure side near the leading edge (T) and trailing edge (U). Some of the fluid particles near the suction side corner enters the tip gap space only to leave it after turning back to suction side. They usually mix with the weak tip vortex forming near the suction side corner. Figure 8 shows that the outer boundaries of the tip leakage vortex for BS 33 is much smaller than that of BS100 that has three times the tip gap height. The weak tip vortex for this case suddenly turns into pressure side of the channel (U1). The leakage flow reversal shown in the vertical visualization planes Z and T in Figure 7 may form a *secondary reversed leakage vortex* (U2) discharging into the pressure side of the blade near the trailing edge.

Because of the extremely narrow tip gap in BS33, in the trailing edge region where there is almost no potential for leakage; the tip gap flow is turned back into the pressure side of the channel via viscous/turbulent shear action. A comparison of BS100 and BS 33 shows the effective weakening of the tip vortex by just designing the tip gap in an extremely tight manner. Although not practical for actual turbine operation, BS33 forms a baseline case for comparative purposes in this study. It is expected that when the tight clearance of BS33 is used *only* in a very narrow region on top of a partial squealer rim, similar flow physics should contribute to the success of the de-sensitization process. Partial squealer tip visualizations are provided in Part-3 of this paper.

CONCLUSIONS

3D viscous flow simulations of the complex tip leakage flow-field existing in the Axial Flow Turbine Facility (AFTRF) are presented for the baseline tip configuration. Although the experimental study presented in Part-1 provides much insight into the physical understanding of the tip region aerodynamics, there are still many areas of the flow-field in which experiments are extremely difficult to perform.

The leakage flow patterns visualized on the baseline tip result in a stage exit total pressure field that is highly comparable to the measurements presented in Part-1. More details on this comparison is provided in Part-3.

Fine details of the entrance flow near the pressure side corner where the tip leakage jet starts to form, the leakage jet formation between the pressure side and the suction side, the re-circulatory flow zone near the pressure side corner in the tip gap zone, the interaction area of the tip vortex with the conventional passage vortex system, the influence of the relative motion of the outer casing and leakage flow reversal can all be visualized in great detail by using computational tools solving the three-dimensional Reynolds Averaged Navier-Stokes Equations. This part of the paper dealing with detailed baseline predictions forms a useful basis for the partial squealer tip visualizations that are presented in Part-3.

The general attributes of the physical aspects of the leakage flows on the baseline tip configuration are successfully simulated in a numerical visualization effort.

The static pressure distributions obtained on the tip platform surface for two different clearance values reveal many important flow features such as low momentum/high static pressure zone near the leading edge, a dominant leakage area near blade mid-chord location and a minimum pressure difference zone between the PS and SS near the trailing edge wedge area.

A strong static pressure modification is apparent when the clearance is reduced to t/h=0.33 % (BS33) from the baseline case of t/h=1.03 % (BS100). The high-pressure zone near the leading edge spread into the mid-chord region of the blade when the clearance is reduced. The velocity vectors in this zone have small magnitude compared to the dominant leakage zone. This high-pressure zone coincides with the central sweet spot observed in cascade heat transfer measurements on similar blades by a number of researchers. Leakage flow paths in this region can be from the pressure side to suction side area as observed from the leakage flow patterns.

Velocity field visualized in planes parallel to the tip platform provides insight in terms of the direction and the magnitude of the leakage flow patterns in the tip gap zone. The viscous/turbulent shearing effect of the outer casing is clearly visible in velocity vector maps especially in the higher plane located very close to the outer casing. When the clearance is tight (BS33), the outer casing viscous/turbulent shear effect is felt even in the lower plane located very near the tip platform of the blade.

A clear visualization of the tip vortex structure for the baseline clearance (BS100) and tight clearance (BS33) is presented in vertical planes (X,Y,Z and T). Vortical flow details in these vertical planes show that a large tip vortex structure rolling near the suction side corner may occupy a large area with significant momentum deficit and energy loss for (BS100). When the clearance is reduced to one third of that of (BS100), an extremely weakened tip vortex structure is visible.

The leakage flow direction, amount and momentum is controlled by the delicate balance between the pressure forces, the shear forces imposed by the outer casing and inertial forces resulting from convective accelerations. It is likely that the shear influence of the outer casing is dominant in blade zones where the driving pressure differentials are minimized by the tip loading conditions.

The numerical visualizations clearly show that the small zone near the leading edge of the blade and the trailing edge wedge zone may have flow leakage from the suction side to pressure side.

Leakage flow reversals in the last 20 % chord of the blade is common. The reversal of the leakage flow occurs in the areas where the driving pressure differential along a leakage flow path between the pressure side and suction side is minimized. The pressure differential is minimal in most turbine blade trailing edge zones because of the highly accelerated passage flows on both sides of the blade are brought into similar Mach number values by design.

The viscous/turbulent shearing effect of the outer casing starts dominating at a much faster rate (earlier chordwise positions) when the clearance is tight.

Strong driving pressure differential in fluid layers near the tip platform and a strong shear force imposed by the outer casing near the outer wall may create sizeable re-circulatory flow patterns in the gap especially in the second half of the blade.

The re-circulatory flow zones numerically visualized in vertical planes form as angular deviations of leakage flow from the mean camber line direction. Flow velocities are such that a typical leakage is sustained from the pressure side to suction side after the mid-chord location. However, in the last 20 % chord of the blade, leakage flow reversal occurs. The leakage flow tends to turn back to the pressure side. Although clearly visible even for the baseline clearance (BS100) case , the reversal of the leakage flow is much stronger for the tight clearance case (BS33).

When tip leakage reversal occurs, some of the fluid trapped inside the conventional tip vortex (located near the suction side corner) may go back into the tip gap zone. This fluid may eventually finds its way to the pressure side. Heat transfer implications of this feature need to be studied since the fluid trapped inside the tip vortex is likely to have higher total temperature than the core flow.

REFERENCES

[1] Liu, J. and Bozzola, R., 1993, Three-Dimensional Navier-Stokes Analysis of Tip Clearance Flow in Linear Turbine Cascades, AIAA Journal, Vol.31, pp.2068-2074.

[2] Basson and Lakshminarayana, 1993, Numerical Simulation of Tip Clearance Effects in Turbomachinery, ASME Journal of Turbomachinery, Vol.109, pp.545-549.

[3] Sell, M., Treiber, M., Casciaro, C. and Gyarmathy, G., Tip-clearance-affected Flow Fields in a Turbine Blade Row, Proc. Inst. Mech. Eng., Vol.213, Part A, pp.309, 318.

[4] Tallman, J. and Lakshminarayana, B., 2001, Numerical Simulation of Tip Leakage Flows in Axial Flow Turbines, with Emphasis on Flow Physics: Part I — Effect of Tip Clearance Height, ASME Journal of Turbomachinery, Vol.123, pp.314-323.

[5] Tallman, J. and Lakshminarayana, B., 2001, Numerical Simulation of Tip Leakage Flows in Axial Flow Turbines, with Emphasis on Flow Physics: Part II — Effect of Outer Casing Relative Motion, ASME Journal of Turbomachinery, Vol.123, pp.324-333.

[6[Ameri, A.A., Steinthorsson, E., Rigby, L.D., 1998, Effects of Tip Clearance and Casing Recess on Heat Transfer and Stage Efficiency in Axial Turbines, Nasa Contract Report NASA/CR-1998-208514.

[7] Bunker, R.S., Bailey, J.C., Ameri, A.A., 2000, Heat Transfer and Flow on the First Stage Blade Tip of a Power Generation Gas Turbine: Part 1-Experimental Results, ASME Journal of Turbomachinery, Vol.122, pp.263-271.

[8] Bunker, R.S., Ameri, A.A., 2000, Heat Transfer and Flow on the First Stage Blade Tip of a Power Generation Gas Turbine: Part 2-Simulation Results, ASME Journal of Turbomachinery, Vol.122, pp.272-277.

[9] Lin, Y.L., Shih, T.I.P., Chyu, M.K. and Bunker, R.S., 2000, Effects of Gap Leakage on Fluid Flow in a Contoured Turbine Nozzle Guide Vane, ASME paper 2000-GT-0555.

[10] Han, S., Han, B., Jin, P. and Goldstein, R.J., 2001, Numerical Prediction of the Flow Field near the Tip of a Rotating Turbine Blade, Jorn. Of Engineering Physics and Thermophysics, Vol.74, No.4, pp.859-868.

[11] Lakshminarayana, B., Camci, C., Halliwell, I., and Zaccaria, M., 1992, "Investigation of Three Dimensional Flow Field in a Turbine Including Rotor/Stator Interaction.
Part I:Design Development and Performance of the Research Facility," AIAA paper 92-3326, presented at the ASME-AIAA Joint Propulsion Conference, Nashville, Tennessee.

[12] Dey, D., Kavurmacioglu, L. and Camci, C., 2002, Aerodynamic Character Of Partial Squealer Tip Arrangements in An Axial Flow Turbine Stage, Part :1 Influence of Partial Squealer Tip Geometry on Measured Aerodynamic Quantities at Stage Exit , paper submitted to ASME IGTI Turbo Expo to be held in Amsterdam, The Netherlands, June 2002.

[13] Launder,B.E. and Spalding,D.B, 1974, The Numerical Computation of Turbulent Flows, Comp.Meth.Appl.Mech. Eng. Vol.3,pp-269-289.

[14] Rains, D.A., 1954, Tip Clearance Flows in Axial Flow Compressors and Pumps, California Inst. of Tech., Hydrodynamics and Mech. Eng. Laboratories, Rep. No. 5.

[15] Morphis, G. and Bindon, J.P., 1988, The Effects of Relative Motion, Blade Edge Radius and Gap Size on the Blade Tip Distribution in an Annular Turbine Cascade with Tip Clearance, ASME paper 88-GT-256.

[16] Dey, D. and Camci, C., 2001 Aerodynamic Tip De-sensitization of an Axial Turbine Rotor Using Tip Platform Extensions, ASME paper 2001-GT-484.